UNIWERSYTET JAGIELLOŃSKI KRAKÓW

ICOLS 03
16th International Conference on Laser Spectroscopy
Palm Cove, Australia

The Structure of Excitation and Fluorescence Spectra Recorded at the $^1 0_u^+ (5^1P_1)$-$X^1 0_g^+$ Transition in Cd_2. Is Cadmium Dimer a van der Waals Molecule? ‡

J. Koperski [a, §], M. Łukomski [a], E. Czuchaj [b] and M. Czajkowski [c]

[a] *Instytut Fizyki, Uniwersytet Jagielloński, ul. Reymonta 4, 30-059 Kraków, Poland*
[b] *Instytut Fizyki Teoretycznej i Astrofizyki, Uniwersytet Gdański, ul. Wita Stwosza 57, 80-952 Gdańsk, Poland*
[c] *Department of Physics, University of Windsor, 401 Sunset Avenue, Windsor, Ontario, N9B 3P4, Canada*

§ *e-mail: ufkopers@cyf-kr.edu.pl, tel.: (+4812) 632-4888 ext. 5789, fax: (+4812) 633-8494*

‡ *supported by the Polish State Committee for Scientific Research (grant 503B 037 20)*

Overview

Excitation and fluorescence ultraviolet spectra of Cd_2 recorded at the $^1 0_u^+(5^1P_1)$-$X^1 0_g^+$ transition are reported. The Cd_2 molecules (seeded in Ar) produced in a continuous free-jet supersonic beam were excited in a vacuum chamber with a pulsed dye-laser beam (Fig. 2). A well-resolved vibrational structure of the $^1 0_u^+ \leftarrow X^1 0_g^+$ excitation spectrum as well as the isotopic structure of the vibrational components were recorded (Figs. 3 and 4). Analysis of the spectrum (Fig. 5) yielded vibrational constants for the $^1 0_u^+$ state: $\omega_e' = 100.50 \pm 0.25$ cm^{-1}, $\omega_e' x_e' = 0.325 \pm 0.003$ cm^{-1}, $D_0' = 8638 \pm 15$ cm^{-1}, $D_e' = 8688 \pm 15$ cm^{-1} and $\Delta R_e = R_e'' - R_e' = 1.04 \pm 0.01$ Å derived for the $^{226}Cd_2$ isotopomer. The $^1 0_u^+$-state potential energy curve was obtained numerically using an inverse perturbation approach procedure [Kosman and Hinze, *J. Mol. Spectrosc.* **56**, 93 (1975), Vidal and Scheingraber, *J. Mol. Spectrosc.* **65**, 46 (1977)] (Fig. 7). A Condon internal diffraction patterns in the $^1 0_u^+ \rightarrow X^1 0_g^+$ fluorescence band, emitted upon a selective excitation of the $\upsilon'=38$ and $\upsilon'=39$ vibrational components of the $^{226}Cd_2$ isotopomer, were observed (Fig. 6) and improved the υ' assignments derived from the analysis of the isotopic structure. Analysis of the fluorescence spectrum yielded information on the repulsive part of the ground-state interatomic potential (Fig. 8). The result confirms a relatively *soft repulsion* between two Cd atoms in the short-range (2.53-4.05 Å) region and make allowance for a *covalent admixture* to the ground-state van der Waals bonding. Quasi-relativistic valence *ab initio* calculations on the potential energy curves for the investigated states have been performed at the complete-active-space multiconfiguration self-consistent-field (CASSCF/CAS) multireference second-order perturbation theory (CASPT2) level with the total 40 correlated electrons. In the calculations, the Cd atom is considered as a 20-valence electron system whereas the Cd^{20+} core is replaced by an energy-consistent pseudopotential which also accounts for scalar-relativistic effects and spin-orbit interaction within the valence shell (Figs. 1, 7 and 8) . A comparison with results of other experiments and *ab initio* calculation is presented.

New Book

J. Koperski
"Van der Waals Complexes in Supersonic Beams. Laser Spectroscopy of Neutral-Neutral Interactions"
Wiley-VCH Verlag, Weinheim, 2003

Here, readers are introduced to the current experimental techniques of laser spectroscopy of van der Waals complexes produced in supersonic beams. The book is unique in its style, subject and scope, and provides information on recent research not only for researchers focusing on molecular spectroscopy but also for those interested in the cooling of atoms and molecules.

From the contents
- *Spectroscopical characterization of weakly bound complexes*
- *Van der Waals interaction*
- *Electronic structure of molecular states*
  - *photoassociation of molecules*
- *Determination of a potential energy curve in different regions of internuclear separations*
- *Experimental considerations - supersonic expansion, source of molecules*
- *12-group homonuclear dimers*
  - *photoassociation and vibrational cooling of Hg_2 molecules in a magneto-optical trap*
- *2-group homonuclear dimers*
- *Metal-rare gas heteronuclear dimers*

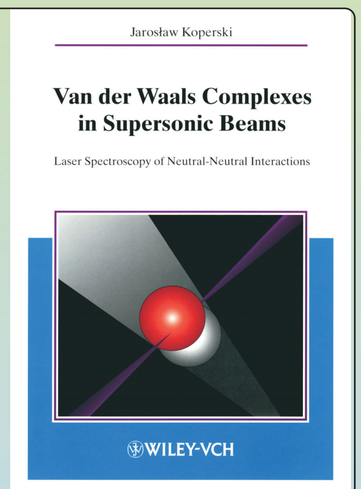

Cd_2 - Result of *ab initio* Calculation

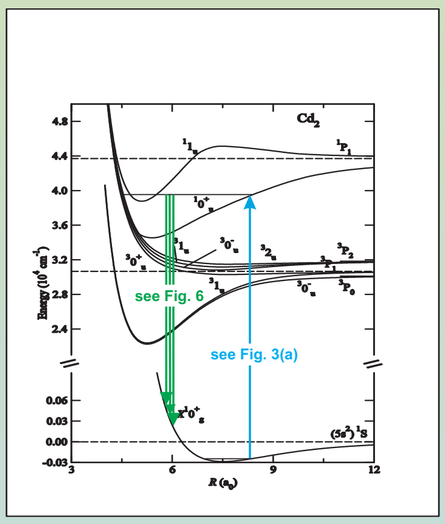

Fig. 1. Ground and Ω-ungerade potential energy curves of Cd_2 molecule obtained in quasirelativistic valence *ab initio* calculations at the complete-active-space multiconfiguration self-consistent-field (CASSCF/CAS) multireference second-order perturbation theory (CASPT2) level with the total 40 correlated electrons. In the calculations, the Cd atom was considered as a 20-valence electron system whereas the Cd^{20+} core is replaced by an energy-consistent pseudopotential which also accounts for scalar-relativistic effects and spin-orbit interaction within the valence shell. The investigated $^1 0_u^+ (5^1P_1) \leftarrow X^1 0_g^+$ and $^1 0_u^+ (5^1P_1) \rightarrow X^1 0_g^+$ transitions are indicated (blue and green arrows, respectively).

Experimental Setup

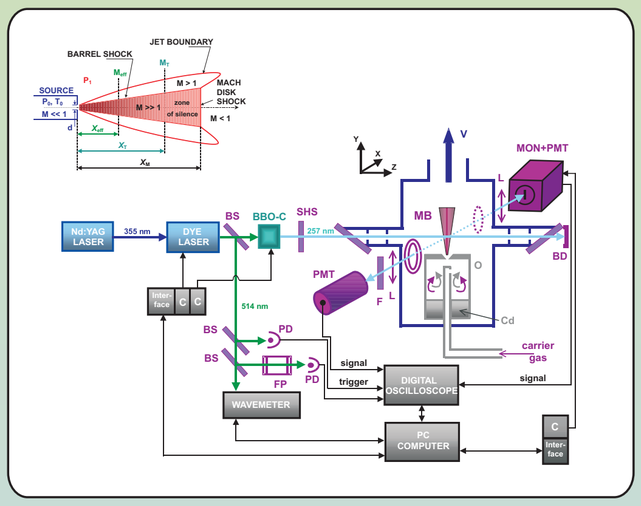

Fig. 2. Schematic layout of the apparatus [see also J. Koperski, *Phys. Reports* **369**, 177(2002)]. **O**-stainless-steel oven; **MB**-molecular beam; **V**-vacuum pump system; **BBO-C**-second harmonic generator; **BS**-beam splitter; **SHS**-second harmonic selector; **C**-scanning controllers; **FP**-Fabry-Perot interferometer; **PD**-photodiodes; **PMT**-photomultiplier tube; **MON**-monochromator; **F**-filter; **L**-lens; **BD**-beam dump. Insert shows schematic diagram of a supersonic expansion beam cross-section. M appropriate Mach numbers: M_{eff} - effective, M_T - terminal; X_{eff}, X_T - corresponding distances from the nozzle; X_M - distance to the Mach disk shock; P_0, T_0, n_0 - pressure, temperature, and density of expanding species in the source; D - diameter of the orifice; P_1 - background pressure ($P_1 << P_0$). Magnitudes of the Mach number (M<<1, M<1, M=1, M>>1) are indicated along the expansion.

Cd_2 Excitation Spectrum Recorded at the $^1 0_u^+(5^1P_1) \leftarrow X^1 0_g^+(5^1S_0)$ Transition

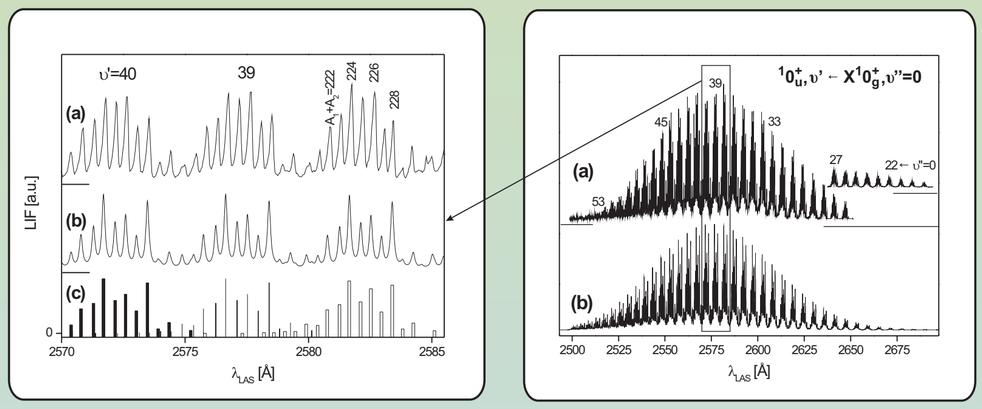

Fig. 3. The $^1 0_u^+, \upsilon' \leftarrow X^1 0_g^+, \upsilon''=0$ transition in an excitation spectrum of Cd_2. **(a)** Experimental trace showing υ' assignments. Effective distance from the nozzle X_{eff}=6 mm, pressure of the carrier gas p_{Ar}=12 atm, temperature of the source oven T_0=870 K, n_0 density number of Cd atoms in the source oven $n_0 = 6 \times 10^{17}$ cm^{-3}, and the density number in the region of excitation n(X_{eff}= 6 mm)=10^{13} cm^{-3}. Laser dye: Coumarine 500 (the long-wavelength part of the spectrum was recorded in a separate experiment with Coumarine 540A). **(b)** Computer-simulated spectrum [LEVEL 7.5 code of R. J. LeRoy, *A Computer Program for Solving the Radial Schrödinger Equation for Bound and Quasibound Levels*, University of Waterloo Chemical Physics Research Report CP-655R, 2002 (unpublished)] showing the "best fit" to the $\upsilon' \leftarrow \upsilon''=0$ progression obtained for $\Delta R_e = 1.04 \pm 0.01$ Å; the simulation includes the isotopic composition of each vibrational component assuming turning-point pairs from the inversive perturbation approach procedure and Morse representations for the excited and ground states, respectively; the relative positions of the isotopic peaks were calculated using Eq. (2), and their amplitudes were weighted relative to the total relative abundances of particular isotopes in natural cadmium. The individual (A_1+A_2) isotopic peaks were represented by a Lorentzian curve with FWHM of 2.3 cm^{-1}. The rotational structure of the isotopic components was not simulated. Details of the υ'=38-40 components (rectangular) are shown in the left part of the Figure. **(c)** Amplitudes of all elementary components with different (m_1+m_2) mass combinations within each of the (A_1+A_2) isotopic peak showing complexity of one vibrational component and drawn in order to show their overlap for neighboring υ'.

Isotopic Structure of the υ'=40 Component

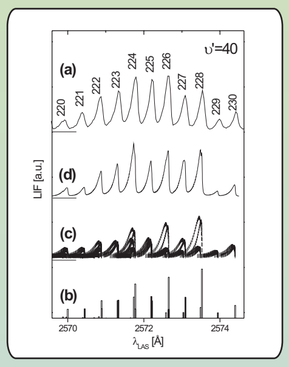

Fig. 4. The isotopic structure of the υ'=40 vibrational component of the spectrum from Fig. 3. **(a)** Experimental trace, (A_1+A_2) for isotopic components are depicted. **(b)** Amplitudes of all elementary components with different (m_1+m_2) mass combinations within each of the (A_1+A_2) isotopic peak showing complexity of one vibrational component. **(c)** Simulation of the rotational structure of each of the (m_1+m_2) elementary component (P and R branches, Q branch is not present); $B_{\upsilon'=40}$=0.0208 cm^{-1} and $B_{\upsilon''=0}$=0.0136 cm^{-1} rotational constants were calculated using formula

$$B_\upsilon = h\,[1-\omega_e x_e(\upsilon+1/2)/\omega_e]/8\pi^2 c\mu R_e^2 \quad , \qquad (1)$$

where h and c are Planck constant and speed of light, respectively, R_e, ω_e and $\omega_e x_e$ are taken from Tables I and II; dependencies $B_e^{isot} = \rho^2 B_e$ and $\alpha_e^{isot} = \rho^3 \alpha_e$, where subscript *isot* denotes the constant for different isotopomer, as well as missing of every alternate line in the branches for each A-like isotopomer and intensity alteration that depends on the statistics of the nuclei were not taken into account as negligible in this approximation; to clarify the picture each rotational component is represented by short vertical line. **(d)** Final simulation obtained by representing each of the rotational components in (c) with a Lorentzian curve with FWHM of 0.3 cm^{-1}.

Analysis of the Excitation Spectrum Recorded at the $^1 0_u^+(5^1P_1) \leftarrow X^1 0_g^+(5^1S_0)$ Transition: Birge-Sponer Plot and Isotopic Shift Analyses

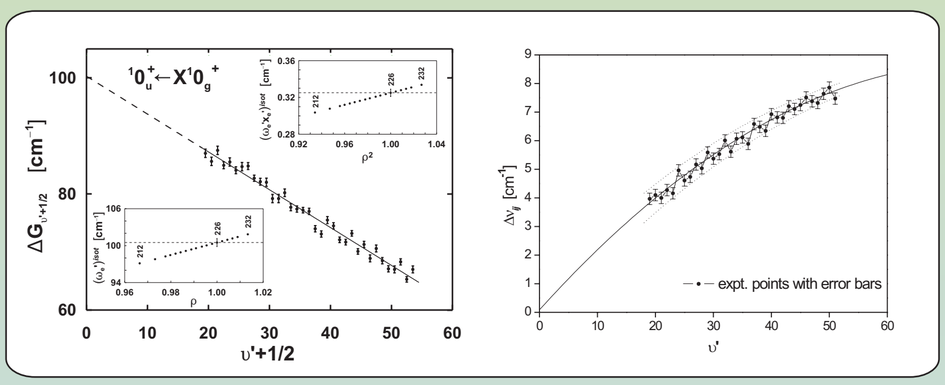

Fig. 5. ***Left:*** Birge-Sponer plot drawn for isotopic peaks belonging to the $^{226}Cd_2$ isotopomer in the $\upsilon' \leftarrow \upsilon''=0$ progression of the excitation spectrum recorded at the $^1 0_u^+ (5^1P_1) \leftarrow X^1 0^+ g$ transition in Cd_2. Dashed line represents a "short" extrapolation which enabled to determine the ω_0' (an intercept with vertical axis). Upper and lower inserts show $\omega_e' x_e' (\rho^2)$ and $\omega_e' (\rho)$ dependencies, respectively, drawn for all different ((A_1+A_2) from 212 to 232) isotopic combinations. ***Right:*** The measured (full circles with error bars), and calculated for υ' (our assignment, solid line) and $\upsilon'\pm3$ (dotted lines) isotopic shifts $\Delta\nu_{ij}$ (see formula below) between different isotopic components in the $^1 0_u^+ \leftarrow X^1 0_g^+$ excitation spectrum of Cd_2 shown in Fig. 3(a). An expression for isotope shift, $\Delta\nu_{ij}$, in $\upsilon' \leftarrow \upsilon''=0$ vibronic transitions between components corresponding to the various (m_1+m_2) combinations of the isotope masses present in natural elements of the molecule is expressed as:

$$\Delta\nu_{ij}(\upsilon') = (1-\rho)\omega_e'(\upsilon'+1/2) - (1-\rho^2)\omega_e' x_e' (\upsilon'+1/2)^2 - (1-\rho)\omega_e''/2 + (1-\rho^2)\omega_e'' x_e''/4 \quad , \qquad (2)$$

where $\rho = (\mu/\mu_j)^{1/2}$ and $\mu = m_1 m_2/(m_1+m_2)$.

Cd_2 Fluorescence Spectrum Recorded at the $^1 0_u^+(5^1P_1) \rightarrow X^1 0_g^+(5^1S_0)$ Transition

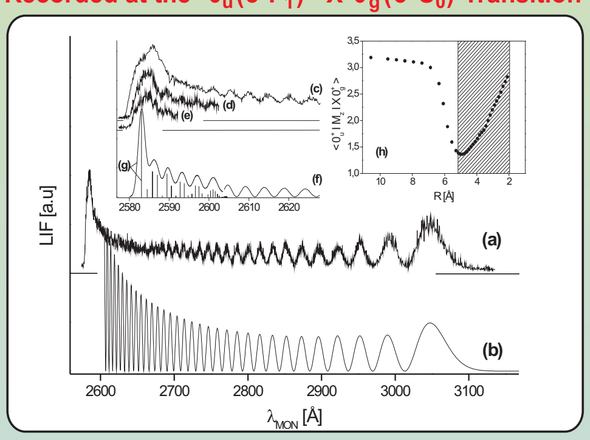

Fig. 6. (a) The total $^1 0_u^+, \upsilon'=38 \rightarrow X^1 0_g^+$ fluorescence band recorded with a 40 cm^{-1} MON slit-width; X_{eff}=4 mm, p_{Ar}=14 atm, T_0=890 K. The sharp peak at the short-wavelength end of the band is due to the $\upsilon'=38 \rightarrow \upsilon''$ bound-bound transitions. **(b)** A computer simulation [R. J. LeRoy, *Comput. Phys. Comm.* **52**, 383 (1989)] of the bound-free part of the band showing the "best fit" obtained using a short-range Ae^{-bR} Born-Mayer potential with A=6.178×10^7 cm^{-1} and b=3.63 Å^{-1} representing the $X^1 0_g^+$ potential. Left insert shows: **(c)**, **(d)** and **(e)** the short-wavelength part of the fluorescence band recorded with slit-widths of 30 cm^{-1}, 20 cm^{-1} and 15 cm^{-1}, respectively, **(f)** part of the simulation of bound-free profile as in (b), **(g)** the simulation [LeRoy, *LEVEL 7.5*.code] of the bound-bound transitions (the individual F-CF corresponding to vibrational transitions vertical bars are represented by a Gauss convolution function representing the MON throughput with FWHM of 2 Å, *i.e.* approx. 30 cm^{-1}; Right insert shows: **(h)** *ab-initio* points calculated for the elements of transition dipole moment $\langle {}^1 0_u^+ | M_z(R) | X^1 0_g^+ \rangle$, region of R corresponding to the detected fluorescence spectrum is depicted.

Potential Energy Curve of the $^1 0_u^+(5^1P_1)$ State

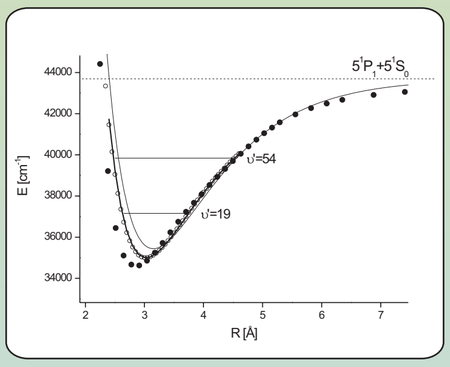

Fig. 7. Potential energy curves for the $^1 0_u^+(5^1P_1)$ state plotted using a Morse representation (thick solid line) with constants obtained in this work (see Table I). Results of the inverse perturbation approach procedure (open circles, the E(R) values are available from the authors (J.K.) upon request) and *ab initio* calculations (full circles) are also shown. A range of υ' levels accessible in the excitation from the $\upsilon''=0$ ground-state level is indicated. The results are compared with a Morse representation (thin solid line) obtained by Rodriguez and Eden [*J. Chem. Phys.* **95**, 5539 (1991)].

Potential Energy Curve of the $X^1 0_g^+(5^1S_0)$ State

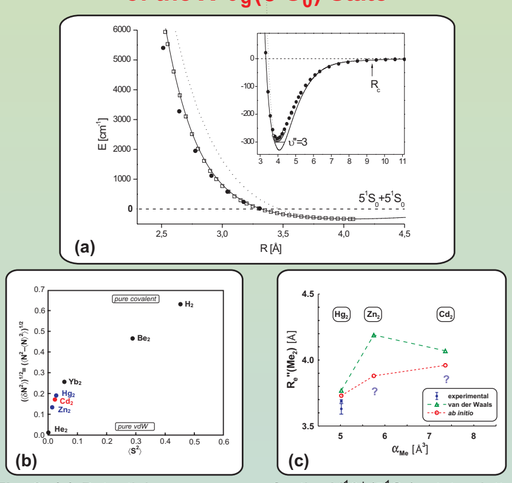

Fig. 8. (a) Potential energy curves for the $X^1 0_g^+(5^1S_0)$ state plotted using the Morse representation [M. Czajkowski and J. Koperski, *Spectrochim. Acta Part A* **55**, 2221 (1999)] (dotted line) as well $Ae^{-bR}+C$ Born-Mayer potential with A=6.178×10^7 cm^{-1}, b=3.63 Å^{-1} and C= -362.91 cm^{-1} (solid line); repulsive part produced by the inversion procedure [R. J. LeRoy, *RPOT* code] (empty squares); points of our *ab initio* calculation (full circles); *ab initio* result of Yu and Dolg [*Chem. Phys. Lett.* **273**, 329 (1997)] (empty circles). The insert shows details of the bound part of the potential: all representations as in main Figure, except a hybrid potential (solid line), *i.e.* the Born-Mayer combined with Morse-vdW potential

$$[D_e''\{1-\exp[-\beta(R-R_e)]\}^2 - \{1-\exp[-(R-R_c)^{12}]\}C_6''/R^6]$$

plotted with D_e''=330.5 cm^{-1}, β=1.1531 Å^{-1}, R_e'' =4.07 Å, C_6'' =2.46106 cm^{-1}Å^6, and R_c=9.34 Å determined in this work. Position of the $\upsilon''=3$ vibrational level is shown. **(b)** Charge fluctuations *versus* square of the local spin for n*s* and n*p* localized valence orbitals on one of the two atoms of several Me_2 dimers. The limiting value of the charge fluctuation is 0.707 for a covalent single bond, whereas a pure vdW interaction corresponds to a value of zero. The square of the local spin is zerofor S=0 and 0.866 for S=1/2. **(c)** Experimental theoretical van der Waals and ab initio ground-state bond lengths, R_e'' plotted versus α_{Me}, for Me_2 (Me=Zn, Cd, Hg) molecules (for details see book advertised in the upper-right corner of the poster.

Table I: Characteristics of the $^1 0_u^+(n^1P_1)$ State in Zn_2, Cd_2 and Hg_2

(all in [cm^{-1}] unless stated otherwise; note: $\Delta R_e = R_e'' - R_e'$)

	Zn_2 (n=4)	Cd_2 (n=5)	Hg_2 (n=6)
ω_0'	-	100.20±0.25 [a,b]	-
ω_e'	122±10 [h]	100.50±0.25 [a,b] 101.2 [f] 105.3±1.0 [i]	79.0±1.0 [j]
$\omega_e' x_e'$	0.40±0.04 [h]	0.325±0.003 [a,b] 0.44±0.03 [i]	0.29556±2×10^5 [j]
D_0'	-	8643±15 [a,c]	8236±15 [k]
D_e'	9010±200 [h]	8693±15 [a,d] 9153 [f] 8250±200 [h]	8280±15 [k]
ΔR_e [Å]	-	1.04±0.01 [a] 0.95±0.02 [h,i]	0.84±0.01 [k]
R_e' [Å]	-	3.03±0.01 [a,e]	2.86 [f] 2.8506 j
ν_{00}	-	35368.8±0.2 [a,b]	46201.7 [k]
B_e'	-	0.0246 [a,g]	0.020542±1×10^6 [j]

[a] this work, derived for the $^{226}Cd_2$ isotopomer
[b] this work, Birge-Sponer plot
[c] this work, from $D_0' = \nu_{00} - \omega_e' + D_e''$
[d] this work, from $D_e' = D_0' + \omega_e'/2 - \omega_e' x_e'/4$
[e] this work, simulation of the $^1 0_u^+ - X^1 0_g^+$ excitation spectrum
[f] this work, *ab initio* calculation
[g] this work, calculated as described in caption of Fig. 4
[h] G. Rodriguez and J. G. Eden, *J. Chem. Phys.* **95**, 5539 (1991)
[i] H. C. Tran and J. G. Eden, *J. Chem. Phys.* **105**, 6771 (1996).
[j] W. Kedzierski et al., *J. Mol. Spectrosc.* **173**, 510 (1995), derived for the $(^{202}Hg)_2$ isotopomer

Table II: Characteristics of the $X^1 0_g^+(n^1S_0)$ State in Zn_2, Cd_2 and Hg_2

(all in [cm^{-1}] unless stated otherwise; note: $\Delta R_e = R_e'' - R_e'$)

	Zn_2 (n=4)	Cd_2 (n=5)	Hg_2 (n=6)
ω_e''	25.9±0.2 [g]	23.0 [g] 20.0 [l], 19.2 [d]	19.6±0.3 [h]
$\omega_e'' x_e''$	0.60±0.05 [g]	0.40±0.01 [g]	0.26±0.05 [h]
D_e''	279.1 [g]	330.5 [g] 290.0 [l], 287.3 [d]	380±15 [h]
R_e'' [Å]	4.19 [g] 3.88 [f], 4.12 [p]	4.07 [g] 3.96 [l], 3.98 [d]	3.77 [g] 3.73 [l], 3.94 [s] 3.63±0.04 [q] 3.69±0.01 [h]
n	-	7.36 [e] 4.45±0.02 [a,f]	6.53 [h, i] 6.21±0.03 [h, j]
B_e''	-	0.0137 [a,c]	0.0123±0.0001 [k]

[a] this work, derived for the $^{226}Cd_2$ isotopomer
[b] this work, simulation of the $^1 0_u^+, \upsilon' \rightarrow X^1 0_g^+$ fluorescence spectrum, where υ'=38 or 39
[c] this work, calculated as described in caption of Fig. 4
[d] this work, *ab initio* calculation
[e] this work, calculated
[f] this work, simulation of the $^1 0_u^+, \upsilon' \rightarrow X^1 0_g^+$ fluorescence spectrum, where υ'=38 or 39
[g] M. Czajkowski and J. Koperski, *Spectrochim. Acta, Part A* **55**, 2221 (1999); theoretical vdW values
[h] J. Koperski *et al.*, *J. Mol. Spectrosc.* **184**, 300 (1997), derived for the $^{401}Hg_2$ isotopomer; expt. values.
[i] J. Koperski *et al.*, *J. Mol. Spectrosc.* **184**, 300 (1997), calculated
[j] J. Koperski *et al.*, *J. Mol. Spectrosc.* **184**, 300 (1997), simulation of the $G^1 0_u^+$, υ'=39 $\rightarrow X^1 0_g^+$ fluorescence spectrum
[k] W. Kedzierski *et al.*, *J. Mol. Spectrosc.* **173**, 510 (1995), derived for the $(^{202}Hg)_2$ isotopomer
[l] M. Yu and M. Dolg, *Chem. Phys. Lett.* **273**, 329 (1997); *ab initio* values.
[m] Slater-Kirkwood formula (J. C. Slater and J. G. Kirkwood, *Phys. Rev.* **37**, 682 (1931)) with correction of R. Cambi *et al.*, *J. Chem. Phys.* **95**, 1853 (1991).
[n] T. Grycuk *et al.*, *Acta Phys. Polon. A* **101**, 825 (2002).
[o] D. Göbel and U. Hohm, *Phys. Rev. A* **52**, 3691 (1995).
[q] R. D. van Zee *et al.*, *Chem. Phys. Lett.* **158**, 306 (1989); expt. values.
[p] E. Czuchaj *et al.*, *Chem. Phys. Lett.* **255**, 203 (1996); *ab initio* values.
[r] F. Schautz *et al.*, *Theor. Chem. Acc.* **99**, 231 (1998); *ab initio* values.
[s] E. Czuchaj *et al.*, *Chem. Phys. Lett.* **214**, 277 (1997); *ab initio* values.
[t] M. Dolg and H.-J. Flad, *J. Phys. Chem.* **100**, 6147 (1996); *ibid.* **100**, 6152 (1996); *ab initio* values.